Наносистеми, наноматеріали, нанотехнології
Nanosistemi, Nanomateriali, Nanotehnologii
2025, т. 23, № 1, сс. 37–60
https://doi.org/10.15407/nnn.23.01.0037

PACS numbers: 68.43.Bc, 71.15.Mb, 71.15.Nc, 73.20.Hb, 76.60.-k, 88.30.R-, 88.40.fh

Stating the Progress of Mn-Based Nanohybrid Materials Containing GaN/AlGaN/InGaN Towards Remarkable Improvement in Hydrogen Storage

Fatemeh Mollaamin

Faculty of Engineering and Architecture,
Department of Biomedical Engineering,
Kastamonu University,
Kastamonu, Turkey

A comprehensive investigation on hydrogen grabbing by heteroclusters of Mn-doped GaN, AlGaN, InGaN is carried out using DFT computations at the CAM–B3LYP–D3/6–311+G(*d*,*p*) level of theory. The notable fragile signal intensity close to the parallel edge of the nanocluster sample might be owing to manganese binding-induced non-spherical distribution of Mn@GaN, Mn@AlGaN or Mn@InGaN heteroclusters. The hypothesis of the energy-adsorption phenomenon is confirmed by density distributions of CDD, TDOS/PDOS/OPDOS, and electron-localization function (ELF) for GaN and its alloys. Based on TDOS, the excessive growth technique on doping manganese is a potential approach to designing high-efficiency hybrid semi-polar gallium nitride-based devices in a long-wavelength zone. A vaster jointed area engages by an isosurface map for Mn-doping GaN, AlGaN, and InGaN towards formation of nanocomposites of Mn@GaN–H, Mn@AlGaN–H, and Mn@InGaN–H after hydrogen adsorption due to labelling atoms of N_4, Mn_5, H_{18}, respectively. Therefore, it can be considered that manganese in the functionalized Mn@GaN, Mn@AlGaN or Mn@InGaN might have more impressive sensitivity for accepting the electrons in the process of hydrogen adsorption. Furthermore, Mn@GaN, Mn@AlGaN or Mn@InGaN are potentially advantageous for certain high-frequency applications requiring solar cells for energy storage. The advantages of manganese over GaN, AlGaN, or InGaN include its higher electron and hole mobility, allowing manganese-doping devices to operate at higher frequencies than non-doping devices.

Комплексне дослідження захоплення Гідроґену гетерокластерами леґованого Mn GaN, AlGaN, InGaN було проведено за допомогою ТФП-обчислень на рівні теорії CAM–B3LYP–D3/6–311+G(*d*,*p*). Помітна інтенсивність нетривкого сиґналу поблизу паралельного краю зразка нанокластера може бути наслідком індукованого зв'язувальним манґаном

несферичного розподілу гетерокластерів Mn@GaN, Mn@AlGaN або Mn@InGaN. Гіпотезу про явище адсорбції енергії було підтверджено розподілами густини CDD, TDOS/PDOS/OPDOS та функції локалізації електронів для GaN та його стопів. Заснований на TDOS, метод надмірного росту за леґування манґаном є потенційним підходом щодо розробки високоефективних гібридних напівполярних пристроїв на основі нітриду Ґалію в довгохвильовій зоні. Більш широку з'єднану область задіяно картою ізоповерхні для леґування Mn GaN, AlGaN, InGaN задля утворення нанокомпозитів Mn@GaN–H, Mn@AlGaN–H, Mn@InGaN–H після адсорбції Гідроґену внаслідок міченння атомів N_4, Mn_5, H_{18} відповідно. Таким чином, можна вважати, що манґан у функціоналізованих Mn@GaN, Mn@AlGaN або Mn@InGaN може мати більш виразну чутливість до прийому електронів у процесі адсорбції Гідроґену. Крім того, Mn@GaN, Mn@AlGaN або Mn@InGaN є потенційно вигідними для певних високочастотних застосувань, які вимагають сонячних елементів для зберігання енергії. Переваги манґану перед GaN, AlGaN або InGaN включають його вищу рухливість електронів і дірок, що уможливлює леґованим манґаном пристроям працювати на вищих частотах, аніж нелеґованим пристроям.

Key words: solar cells, hydrogen adsorption, energy storage, aluminium–gallium nitride, indium gallium nitride, first-principles study.

Ключові слова: сонячні батареї, адсорбція Гідроґену, накопичення енергії, нітрид Алюмінію–Ґалію, нітрид Ґалію–Індію, першопринципне дослідження.

(Received 23 October, 2024; in revised form, 25 October, 2024)

1. INTRODUCTION

A binary III/V direct bandgap semiconductor called gallium nitride (GaN) is a very hard material with wide bandgap applied in a variety of technologies, including optoelectronic, high-power electronics and light-emitting diodes, partly due to its favourable thermal properties [1, 2].

The nitrides of group III in periodic table have low sensitivity to ionizing radiation that makes them appropriate materials for solar cell arrays for satellites. Therefore, space applications could also benefit as devices have shown stability in high radiation environments.

Ternary 'AlGaN' alloys have been recognized as promising materials for realizing deep ultraviolet 'DUV' optoelectronic devices with operating wavelengths down to 200 nm [1–3]. For the development of high performance AlGaN-based 'DUV' devices, high-conductivity *p*-type Al-rich $Al_xGa_{1-x}N$ ($x \geq 0.4$) is essential. Many studies have shown that enhancing the *p*-type conductivity has a

significant effect on the improvement of both the electrical and optical properties of AlGaN DUV optoelectronics [4–8]. In an investigation, the scientists have shown the $Al_{0.1}Ga_{0.9}N/GaN$ heterojunction solar cells with a Mn-doped active layer. Under a 1-sun AM1.5 G illumination condition, the devices exhibited improved conversion efficiency by a magnitude of 5 compared to the cells without Mn doping in the active layer. This dramatic increase in conversion efficiency is attributed to the fact that the Mn-related energy states cause sub-band gap photon absorption and thereby contribute an extra photocurrent [9]. The investigations conducted on Mn-doped GaN have shown that the Mn impurity band could form approximately at the middle of the GaN band gap [10] (Fig. 1).

The researchers have estimated the suitability of Mn doped $In_{1-x}Ga_xN$ as an IB material. They predicted that the $In_{1-x}Ga_xN$-based solar cells with a Mn-doped absorption layer could achieve maximum efficiency [11].

The ternary semiconductor of Indium gallium nitride (InGaN) as solar cells is remarkable owing to the adjustable direct band gap energy of InGaN veiling the total solar spectrum arraying from 0.7 to 3.4 eV [12, 13], as well as preferable photovoltaic specifics of InGaN consisting of vast absorption coefficients [14] and high carrier dynamism. Furthermore, great fixity and excellent radiation persistence of InGaN alloys permit function of InGaN-based instruments in uttermost situations such as space and geocentric usages

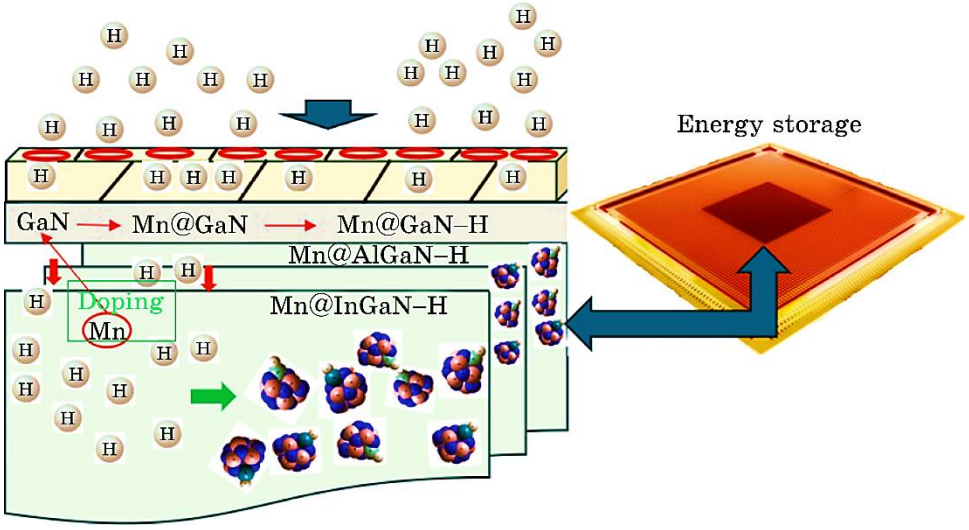

Fig. 1. Application of Mn-doped hetero-clusters of GaN, AlGaN, InGaN for hydrogen storage in transistors using CAM–B3LYP–D3/6-311+G(*d*,*p*) calculation (@ denotes doping).

[12, 15]. The solar cells of InGaN were constructed with low indium amounts of the InGaN alloy compounds [16–18] that conduces to an enhancement in the band gap energy of InGaN and then eventuates in the absorption of shorter wavelengths of solar radiation. Therefore, to find out InGaN solar cells with high yield, the In amount in the InGaN active layer of these solar cells should be enhanced to compensate a large part of the solar spectrum. Recently, it has been suggested the application of dual nanogratings of Si and other organic solar cells, which are mostly in direct contact with the active area of the solar cells [19–25].

Moreover, the researchers fabricated transition metal zinc doped InGaN nanorods arrays by radio-frequency plasma-assisted molecular beam epitaxy. Doping obviously reduces indium atoms composition, the aggregation of In–In and induces the deep energy level. This greatly decreases the defects and improves the valence band potential of InGaN nanorods [26].

Recently, researchers have proposed an InGaN/GaN *p–i–n* thin-film solar cell, which includes a dual nanograting compound: silver nanogratings on the back of the solar cell and GaN–NGs on the front. FDTD simulation parameters have exhibited that the dual NG compound connects the eventual sunlight to the plasmonic and photonic styles, so enhancing the absorption of the solar cell in a wide spectral span. It is perceived that the solar cells possessing the double nanograting structures have a considerable increment in light absorption compared with cells either having no nanogratings or having only the front nanogratings or only the back nanogratings [27].

In this paper, we propose the feasible semiconductors of GaN, AlGaN, InGaN, which are doped with manganese (Fig. 1). We carried out molecular modelling considering the geometrical parameters of doping atoms on the surface of Mn@GaN, Mn@AlGaN, and Mn@InGaN through hydrogen absorption status and current charge density of the solar cells was studied. Moreover, the effect of a relative chemical shift between GaN, AlGaN, InGaN and doped heteroclusters of the solar cell was also investigated.

2. MATERIALS AND METHODS

The Mn-doped GaN, AlGaN, InGaN nanocomposites were calculated within the framework of first-principles calculation based on density functional theory (DFT) (Fig. 2). The rigid potential energy surface using density functional theory [28–41] was performed due to Gaussian 16 revision C.01 program package [42] and GaussView 6.1 [43]. The coordination input for energy storage on the solar cells has applied 6–311+G(*d*,*p*) and EPR-3 basis sets.

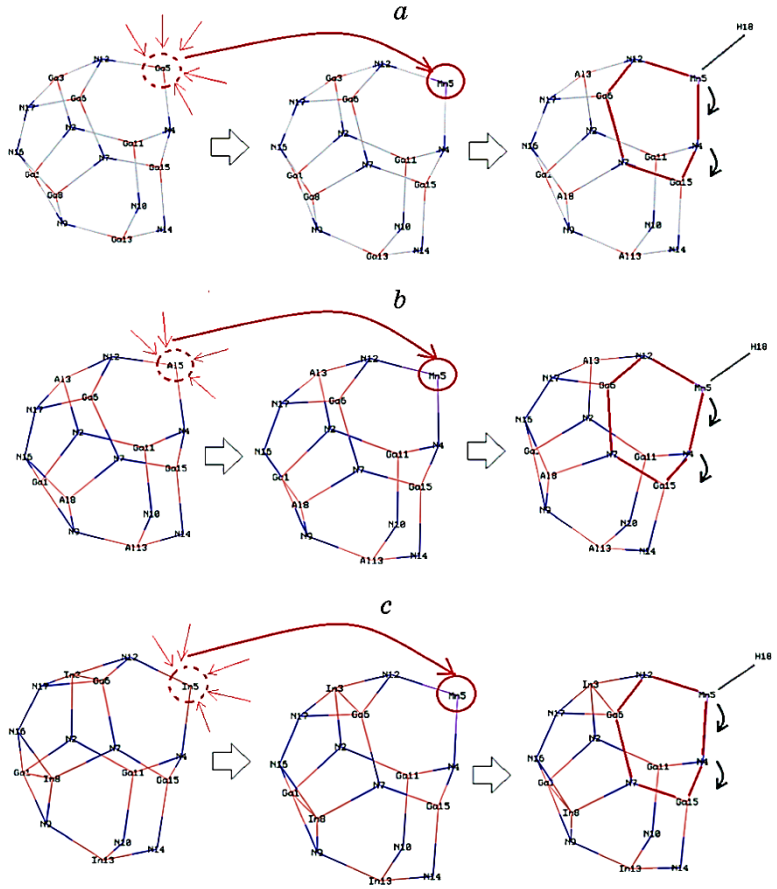

Fig. 2. Characterization of heteroclusters includes (*a*) Mn@GaN/Mn@GaN–H; (*b*) Mn@AlGaN/Mn@AlGaN–H; (*c*) Mn@InGaN/Mn@InGaN–H through a labelled ring in clockwise manner including Mn_5, N_4, Ga_{15}, N_7, Ga_6, N_{12} towards H-adsorption.

First, we optimized the structural parameters of nanoclusters of GaN, AlGaN, InGaN which are doped with manganese towards formation of heteroclusters of Mn@GaN, Mn@AlGaN, Mn@InGaN for obtaining the highest short-circuit current density. Then, Figure 1 shows the process of hydrogen adsorption on heteroclusters of Mn@GaN, Mn@AlGaN, Mn@InGaN, which are varied to maximize the absorption in the active region. This is a utility used to calculate ring area and perimeter, since ring area is sometimes involved in wave-function analysis. In this function, it is needed to input the index of the atoms in the ring in clockwise manner including Mn_5, N_4, Ga_{15}, N_7, Ga_6, N_{12} (Fig. 2, *a*, *b*, *c*). Then, it has be calculated total ring area and total ring perimeter for a tailored ring as 9.6981

Å^2 and 11.6921 Å^2, respectively (Fig. 2, *a*, *b*, *c*).

3. RESULTS AND DISCUSSION

In this article, the data has evaluated the efficiency of metal-doped hybrid nanoalloys of Mn@GaN, Mn@AlGaN, Mn@InGaN and their hydrated complexes of Mn@GaN–H, Mn@AGaN–H, Mn@InGaN–H energy saving in batteries, transistors and solar cells.

3.1. Analysis of CDD, TDOS/PDOS/OPDOS and ELF

The amounts of charge density differences 'CDD' is measured by considering isolated atoms or noninteracting ones. The mentioned approximation can be the lightest to use because the superposition value may be received from the primary status of the self-consistency cycle in the code that carries out the density functional theory (Fig. 3, *a*, *b*, *c*) [44].

Figure 2, *a* indicates the atom of Mn_5 from Mn@GaN and Mn_5, H_{18} from Mn@GaN–H accompanying gallium and nitrogen atoms fluctuating around −9 to +3 Bohr. In Figure 2, *b*, the atom of Mn_5 from Mn@AlGaN and Mn_5, H_{18} from Mn@AlGaN–H accompanying aluminium, gallium and nitrogen atoms have shown the fluctuation around −9 to +3 Bohr and −8 to +4 Bohr, respectively. Moreover, the atom of Mn_5 from Mn@InGaN and Mn_5, H_{18} from Mn@InGaN–H accompanying indium, gallium and nitrogen atoms have shown the fluctuation around −9 to +3 Bohr (Fig. 3, *c*).

To understand better the different adsorption characteristics of Mn@GaN, Mn@GaN–H, Mn@AlGaN, Mn@AlGaN–H, Mn@InGaN, Mn@InGaN–H, total density of states (TDOS) using Multiwfn program [45] has been measured. This parameter can indicate the existence of important chemical interactions often on the convex side (Fig. 4, *a*, *a′*, *b*, *b′*, *c*, *c′*). In isolated system (such as molecule), the energy levels are discrete, the concept of density of state (DOS) is supposed completely valueless in this situation. Therefore, the original total DOS (TDOS) of isolated system can be written as [45]:

$$\mathrm{TDOS}(E) = \sum_i \delta\left(E - \in_i\right), \tag{1}$$

$$G(x) = \frac{1}{c\sqrt{2\pi}} e^{-\frac{x^2}{2c^2}}, \text{ where } c = \frac{FWHM}{2\sqrt{2\ln x}}. \tag{2}$$

Moreover, the curve map of broadened partial DOS (PDOS) and overlap DOS (OPDOS) are valuable for visualizing orbital composition analysis, PDOS function of fragment *A* is defined as

$$\mathrm{PDOS}_A(E) = \sum_i \Xi_{i,A} F\left(E - \in_i\right), \tag{3}$$

where $\Xi_{i,\,A}$ is the composition of fragment A in orbital i. The OPDOS between fragment A and B is defined as:

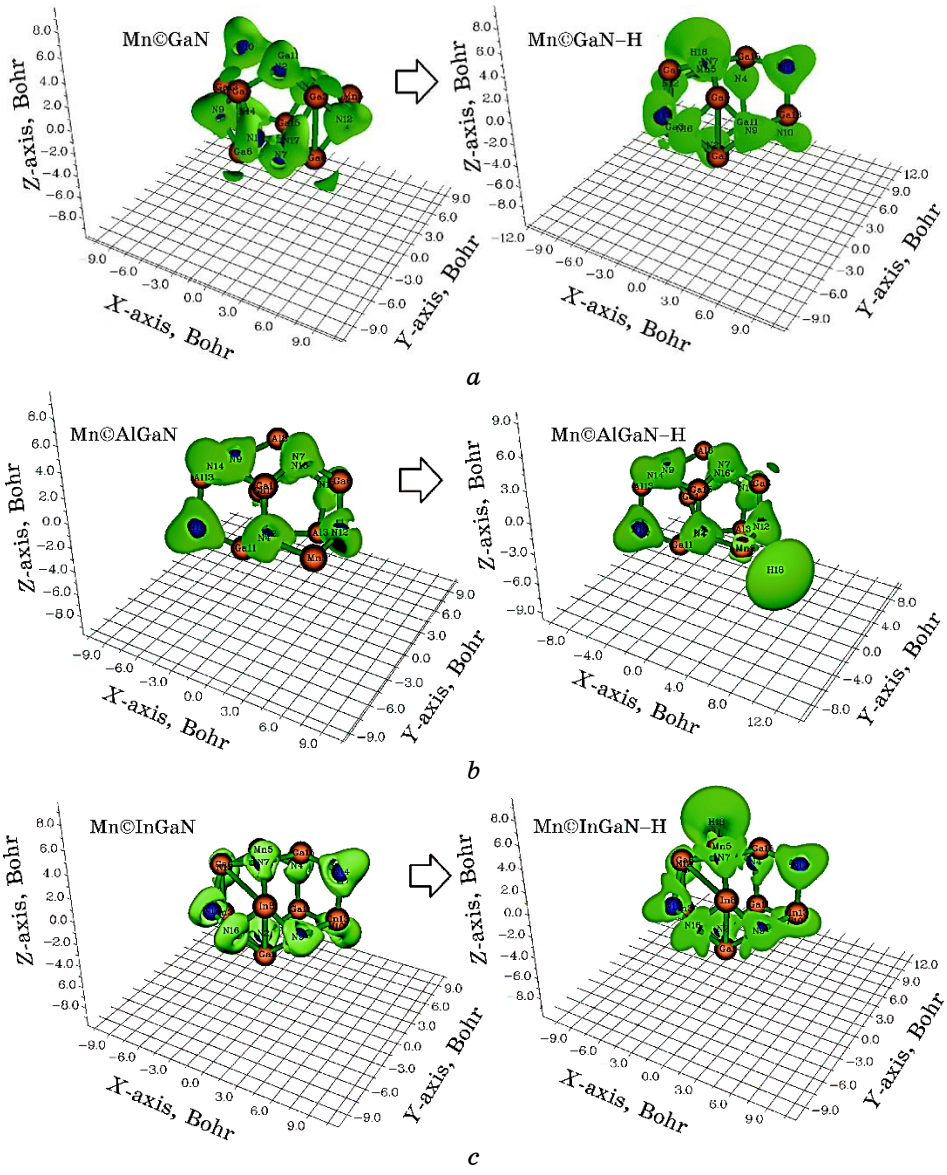

Fig. 3. CDD graphs for heteroclusters through hydrogen adsorption including (*a*) Mn@GaN/Mn@GaN–H, (*b*) Mn@AlGaN/Mn@AlGaN–H, and (*c*) Mn@InGaN/Mn@InGaN–H.

$$\mathrm{OPDOS}_{A,B}(E) = \sum_i X^i_{A,B} F\left(E - \in_i\right), \tag{4}$$

where $X^i_{A,B}$ is the composition of total cross term between fragment A and B in orbital i.

In the TDOS map, each discrete vertical line corresponds to a molecular orbital (MO), the dashed line highlights the position of HOMO. The curve is the TDOS simulated based on the distribution of MO energy levels. In the negative part, the region around −0.40 a.u. has obviously larger state density than other regions for Mn@GaN, Mn@GaN−H, Mn@AlGaN, Mn@AlGaN−H, Mn@InGaN,

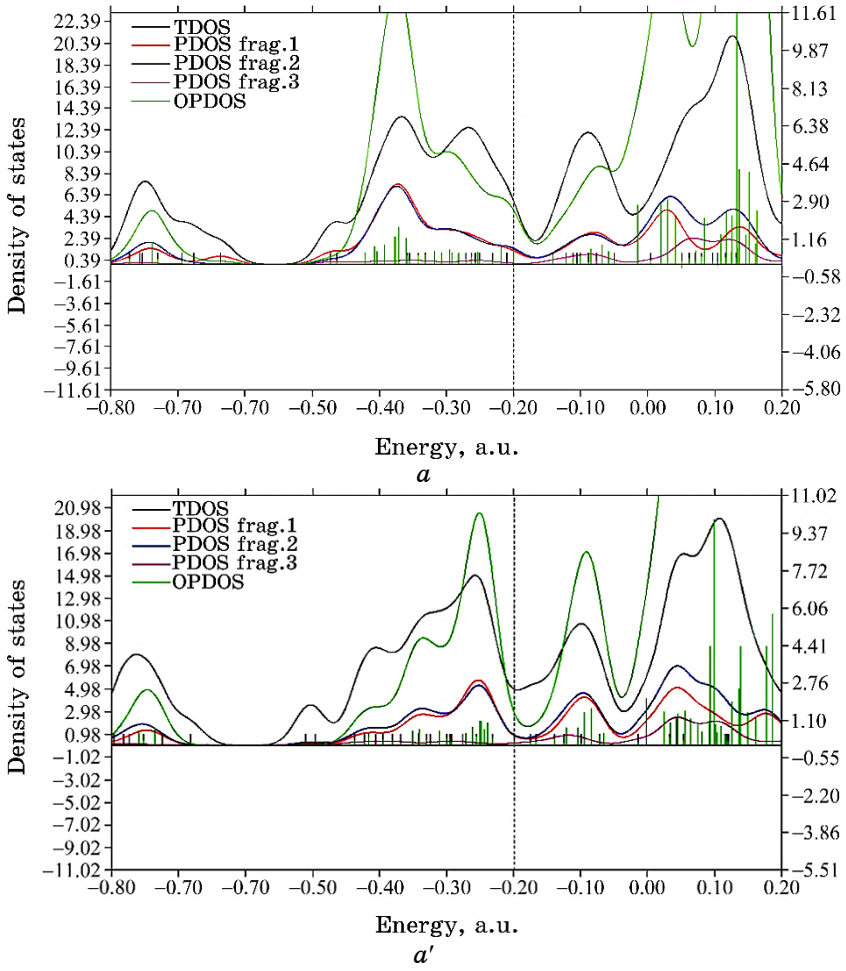

Fig. 4. TDOS/PDOS/OPDOS graphs of heteroclusters include (*a*) Mn@GaN, (*a′*) Mn@GaN−H, (*b*) Mn@AlGaN, (*b′*) Mn@AlGaN−H, (*c*) Mn@InGaN, (*c′*) Mn@InGaN−H.

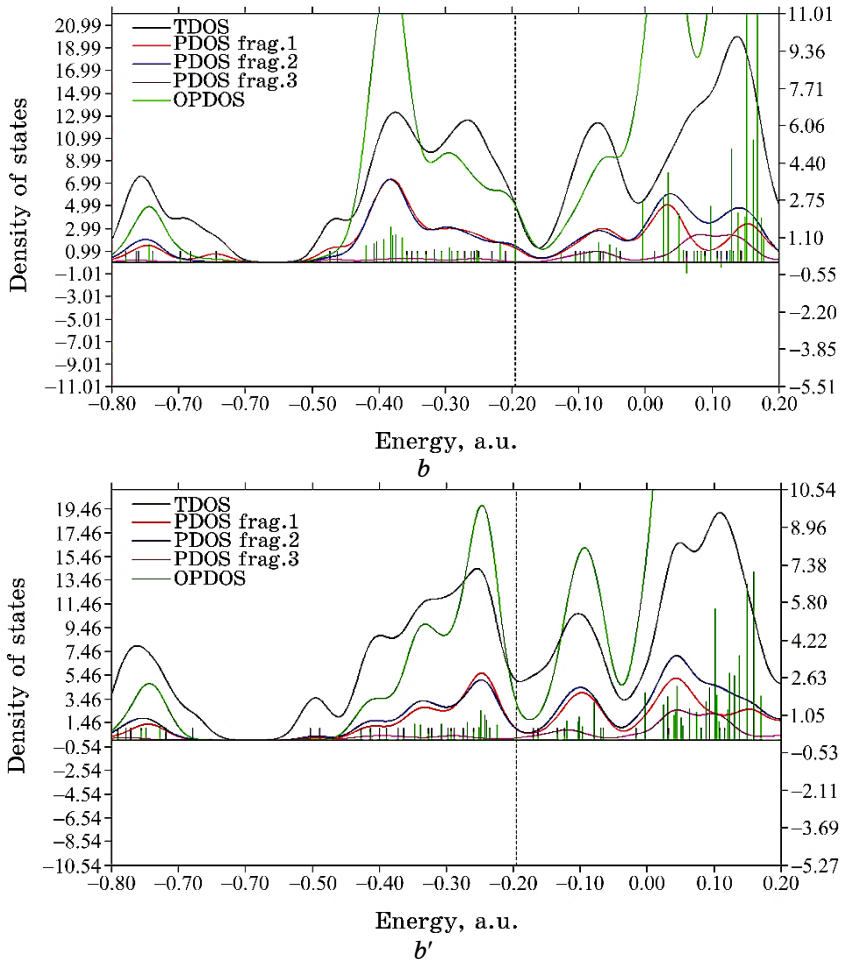

Continuation **Fig. 4.**

Mn@InGaN–H (Fig. 4, *a*, *a′*, *b*, *b′*, *c*, *c′*).

However, Mn@InGaN–H (Fig. 4, *c′*) has shown larger state density through pointed peaks than Mn@GaN–H (Fig. 4, *a′*) and Mn@AlGaN–H (Fig. 4, *b′*). It is remarkable that the excessive growth technique on doping manganese as noble transition metal is a potential approach to designing high efficiency hybrid semi-polar gallium nitride alloys devices on aluminium or indium layers in a long wavelength zone.

Fragment 1 has been defined for N_2, X_3 (X = Ga, Al, In), N_4, Mn_5, Ga_{11}, N_{12}, N_{17} for Mn@GaN (Fig. 4, *a*), Mn@AlGaN (Fig. 4, *b*), Mn@InGaN (Fig. 4, *c*) and H_{18} for Mn@GaN (Fig. 4, *a′*), Mn@AlGaN (Fig. 4, *b′*), Mn@InGaN (Fig. 4, *c′*). Moreover, Fragment 2 has indi-

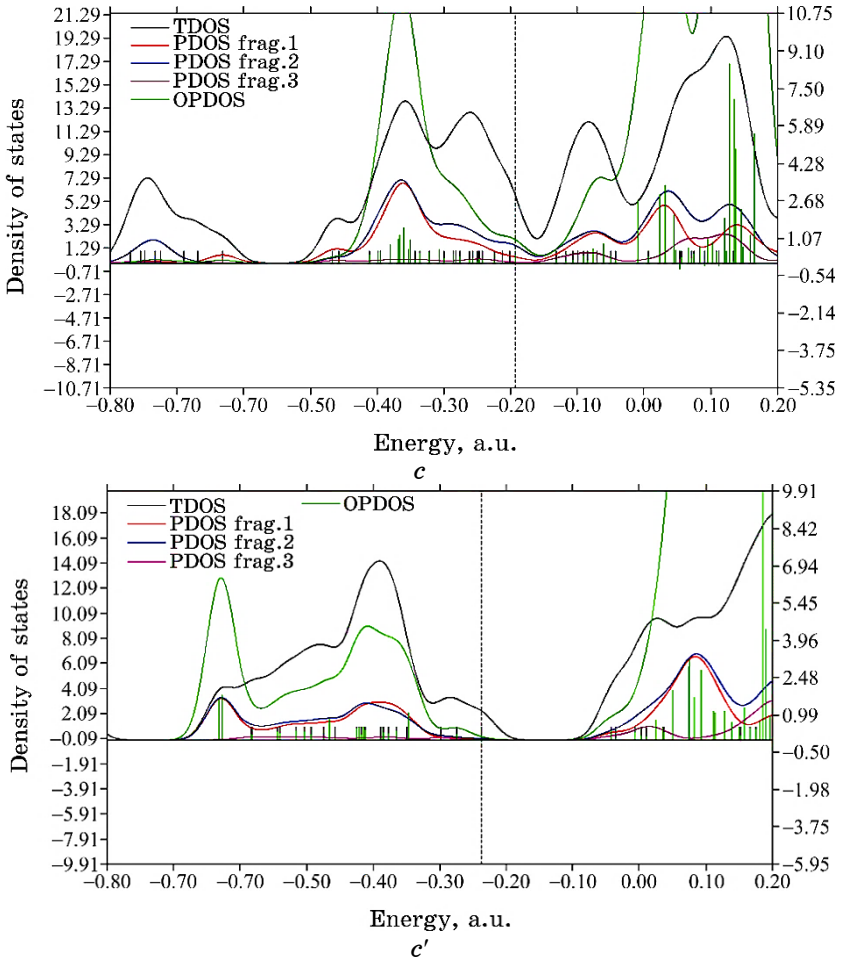

Continuation **Fig. 4.**

cated the fluctuation of N_4, Mn_5, Ga_6, N_{10}, N_{12}, Y_{13} (Y = Ga, Al, In), Ga_{15}, N_{17} for Mn@GaN (Fig. 4, *a*), Mn@AlGaN (Fig. 4, *b*), Mn@InGaN (Fig. 4, *c*) and H_{18} for Mn@GaN (Fig. 4, *a′*), Mn@AlGaN (Fig. 4, *b′*), Mn@InGaN (Fig. 4, *c′*). Finally, it was considered the fluctuation of Ga_1, N_7, Z_8 (Z = Ga, Al, In), N_9, Y_{13} (Y = Ga, Al, In), N_{14}, N_{16}, N_{17} for Mn@GaN (Fig. 4, *a*), Mn@AlGaN (Fig. 4, *b*), Mn@InGaN (Fig. 4, *c*) and H_{18} for Mn@GaN (Fig. 4, *a′*), Mn@AlGaN (Fig. 4, *b′*), Mn@InGaN (Fig. 4, *c′*) through Fragment 3.

Furthermore, a type of scalar fields called electron localization function (ELF) may demonstrate a broad span of bonding samples. Nevertheless, the distinction between deduced/raised electron delocalization/localization into cyclic π-conjugated sets stays encourag-

ing for ELF [46]. The grosser the electron localization is in an area, the more likely the electron movement is restricted within it. Therefore, they might be discerned from the ones away, if electrons are totally centralized. As Bader investigated, the zones with large electron localization possess extensive magnitudes of Fermi hole integration. However, with having a six-dimension function for the Fermi hole, it seems hard to be studied directly. Then, Becke and Edgecombe remarked that spherically averaged as if spin conditional pair probability possesses a direct correlation with the Fermi hole and proposed the parameter of electron localization function (ELF) in Multiwfn program [29] and popularized for spin-polarized procedure [47]:

$$\mathrm{ELF}(r) = \frac{1}{1 + \left[D(r) \,/\, D_0(r)\right]}, \tag{5}$$

where

$$D(r) = \frac{1}{2}\sum\nolimits_i \eta_i \mid \nabla\varphi_i(r) \mid^2 - \frac{1}{8}\left[\frac{\mid \nabla\rho_\alpha(r) \mid^2}{\rho_a(r)} + \frac{\mid \nabla\rho_\beta(r) \mid^2}{\rho_\beta(r)}\right], \tag{6}$$

and

$$D_0(r) = \frac{3}{10}(6\pi^2)^{2/3}\left[\rho_a(r)^{5/3} + \rho_\beta(r)^{5/3}\right]. \tag{7}$$

For close-shell system, since $\rho_\alpha = \rho_\beta = (1/2)\rho$, D and D_0 terms can be simplified as:

$$D(r) = \frac{1}{2}\sum\nolimits_i \eta_i \mid \nabla\varphi_i(r) \mid^2 - \frac{1}{8}\frac{\mid \nabla\rho(r) \mid^2}{\rho(r)}, \tag{8}$$

and

$$D_0(r) = \frac{3}{10}(3\pi^2)^{2/3}\rho(r)^{5/3}. \tag{9}$$

Regarding kinetic energy, ELF was rechecked to be more punctual for both Kohn–Sham DFT and post-HF wave-functions [48]. In fact, the excess kinetic-energy density caused by Pauli repulsion was unfolded by $D(r)$ and $D_0(r)$ and may be inspected as Thomas–Fermi kinetic-energy density. Because $D_0(r)$ is brought forward the ELF as origin, what the ELF shows is affiliate localization. The compounds of Mn@GaN, Mn@GaN–H, Mn@AlGaN, Mn@AlGaN–H, Mn@InGaN, and Mn@InGaN–H can be defined by ELF graphs owing to exploring their delocalization/localization characterizations of electrons and chemical bonds (Fig. 5, *a*, *a*′, *b*, *b*′, *c*, *c*′).

The counter map of ELF for Mn@GaN, Mn@GaN–H (Fig. 5, *a*, *a*′), Mn@AlGaN, Mn@AlGaN–H (Fig. 5, *b*, *b*′), Mn@InGaN, Mn@InGaN–H (Fig. 5, *c*, *c*′) has shown the electron delocalization through a labelled ring in clockwise manner including Mn_5, N_4, Ga_{15}, N_7, Ga_6, N_{12} and H_{18} towards H-adsorption (Fig. 2, *a*, *b*, *c*). Then, hydration of Mn-doped GaN, AlGaN, InGaN indicates a larger isosurface map of electron delocalization due to labelling atoms of N_4, Mn_5, H_{18} in Mn@GaN–H (Fig. 5, *a*′), Mn@AlGaN–H (Fig. 5, *b*′), Mn@InGaN–H (Fig. 5, *c*′).

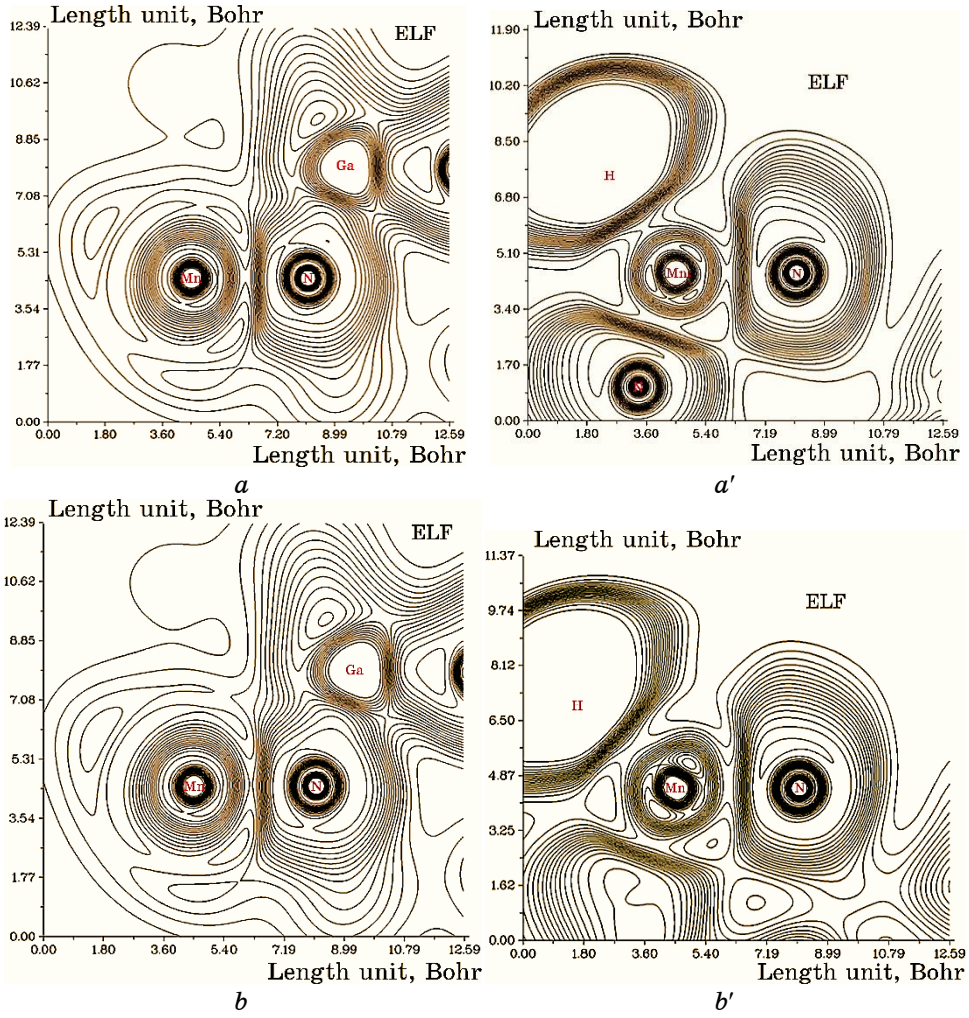

Fig. 5. The graphs of ELF for heteroclusters include (*a*) Mn@GaN/Mn@GaN–H, (*b*) Mn@AlGaN/Mn@AlGaN–H, and (*c*) Mn@InGaN/Mn@InGaN–H.

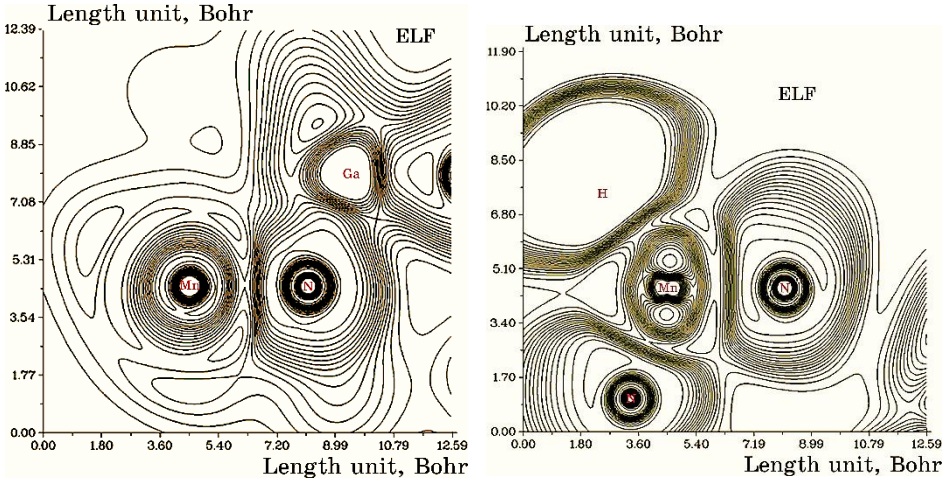

c *c′*

Continuation **Fig. 5.**

A narrower connected area occupied by an isosurface map means that electron delocalization is relatively difficult. However, the large counter map of ELF for Mn@GaN, Mn@AlGaN, and Mn@InGaN can confirm that doping Mn nanoparticles on the surface increases the efficiency of solar cells of GaN, AlGaN, and InGaN for energy storage (Table 1).

Besides, the changes of charge-density analysis have illustrated that GaN, AlGaN, InGaN have shown the Bader charge of –1.092, –1.272, –1.131 coulomb before Mn-doping and –1.048, –1.252, –1.098 coulomb after Mn-doping, respectively, that describes the tensity value of these heteroclusters for energy storage (Table 1).

3.2. Analysis of Nuclear Magnetic Resonance Spectra

Based on the resulted amounts, nuclear magnetic resonance (NMR) spectra of Mn@GaN, Mn@AlGaN, Mn@InGaN heteroclusters as the potential molecules for energy storage can unravel the efficiency of these complexes in solar cells through hydrogen adsorption. From the DFT calculations, it has been attained the chemical shielding (CS) tensors in the principal axes system to estimate the isotropic chemical-shielding (CSI) and anisotropic chemical-shielding (CSA) [49]:

$$\sigma_{\text{iso}} = \left(\sigma_{11} + \sigma_{22} + \sigma_{33}\right) / 3, \tag{10}$$

$$\sigma_{\text{aniso}} = \sigma_{33} - \left(\sigma_{22} - \sigma_{11}\right) / 2. \tag{11}$$

TABLE 1. Data of Bader charge (*Q*/Coulomb) for selected atoms of Mn@GaN, Mn@GaN–H, Mn@AlGaN, Mn@AlGaN–H, Mn@InGaN, Mn@InGaN–H heteroclusters.

Mn@GaN		Mn@GaN–H		Mn@AlGaN		Mn@AlGaN–H		Mn@InGaN		Mn@InGaN–H	
Atom	*Q*	Atom	*Q*	Atom	*Q*	Atom	*Q*	Atom	*Q*	Atom	*Q*
Ga_1	0.9961	Ga_1	1.0084	Ga_1	0.9852	Ga_1	0.9960	Ga_1	0.9511	Ga_1	1.3172
N_2	–1.0483	N_2	–1.0386	N_2	–1.1478	N_2	–1.1288	N_2	–1.0594	N_2	–1.4501
Ga_3	0.9744	Ga_3	0.9936	Al_3	1.2520	Al_3	1.2506	In_3	1.0827	In_3	1.4791
N_4	–1.0171	N_4	–0.9210	N_4	–1.0561	N_4	–0.9446	N_4	–1.0219	N_4	–1.3388
Mn_5	0.7522	Mn_5	0.4224	Mn_5	0.7651	Mn_5	0.3908	Mn_5	0.7195	Mn_5	0.8126
Ga_6	0.9743	Ga_6	0.9933	Ga_6	0.9729	Ga_6	0.9814	Ga_6	0.9420	Ga_6	1.2959
N_7	–1.0482	N_7	–1.0489	N_7	–1.1444	N_7	–1.1129	N_7	–1.0627	N_7	–1.4452
Ga_8	0.9958	Ga_8	1.0123	Al_8	1.2493	Al_8	1.2696	In_8	1.0981	In_8	1.5085
N_9	–1.0455	N_9	–1.0148	N_9	–1.2162	N_9	–1.1616	N_9	–1.0715	N_9	–1.4269
N_{10}	–0.6809	N_{10}	–0.6763	N_{10}	–0.7651	N_{10}	–0.7700	N_{10}	–0.7066	N_{10}	–0.8648
Ga_{11}	1.0012	Ga_{11}	1.0242	Ga_{11}	0.9972	Ga_{11}	1.0024	Ga_{11}	0.9750	Ga_{11}	1.4177
N_{12}	–0.9800	N_{12}	–0.9025	N_{12}	–1.0750	N_{12}	–0.9475	N_{12}	–0.9944	N_{12}	–1.3611
Ga_{13}	0.9259	Ga_{13}	0.9193	Al_{13}	1.2071	Al_{13}	1.1771	In_{13}	1.0188	In_{13}	1.3032
N_{14}	–0.6808	N_{14}	–0.6916	N_{14}	–0.7669	N_{14}	–0.7570	N_{14}	–0.7110	N_{14}	–0.9195
Ga_{15}	1.0012	Ga_{15}	1.0272	Ga_{15}	1.0015	Ga_{15}	1.0088	Ga_{15}	0.9812	Ga_{15}	1.4087
N_{16}	–0.5692	N_{16}	–0.5456	N_{16}	–0.6368	N_{16}	–0.6195	N_{16}	–0.5787	N_{16}	–0.8417
N_{17}	–0.5512	N_{17}	–0.5327	N_{17}	–0.6220	N_{17}	–0.6003	N_{17}	–0.5623	N_{17}	–0.8212
		H_{18}	–0.0285			H_{18}	–0.0345			H_{18}	–0.0735

The NMR data of isotropic (σ_{iso}) and anisotropic shielding tensors (σ_{aniso}) for Mn-doped GaN, AlGaN and InGaN and their hydrated derivatives of Mn@GaN–H, Mn@AlGaN–H, Mn@InGaN–H have been computed by Gaussian 16 revision C.01 program package [26] and been shown in Table 2. The notable fragile signal intensity close to the parallel edge of the nanocluster sample might be owing to manganese binding induced non-spherical distribution of GaN (Fig. 6, *a*) and Mn@AlGaN (Fig. 6, *b*) heteroclusters. Figure 6, *c* exhibited the same tendency of shielding; however, a considerable deviation exists from doping atoms of manganese as electron acceptors on the surface of Mn@InGaN heterocluster.

The observed increase in the chemical shift anisotropy spans for nanocages of Mn@GaN/Mn@GaN–H (Fig. 6, *a*) and Mn@InGaN/Mn@InGaN–H (Fig. 6, *c*) is near N_{10} and N_{14}, and for Mn@AlGaN/Mn@AlGaN–H is close to N_{10}, N_{14}, and N_{17} (Fig. 6, *b*).

TABLE 2. Data of NMR shielding tensors (ppm) for selected atoms of Si–AlGaN, Si–AlGaN–H, Ge–AlGaN, Ge–AlGaN–H, Pd–AlGaN, Pd–AlGaN–H, Pt–AlGaN, Pt–AlGaN–H heteroclusters.

Mn@GaN			Mn@GaN–H			Mn@AlGaN		
Atom	σ_{iso}	σ_{aniso}	Atom	σ_{iso}	σ_{aniso}	Atom	σ_{iso}	σ_{aniso}
Ga_1	10.6772	8.1116	Ga_1	7.8121	31.2686	Ga_1	10.4656	8.1593
N_2	127.8331	150.7727	N_2	11.3237	302.2757	N_2	146.5709	121.3465
Ga_3	8.8962	7.1266	Ga_3	0.0389	103.9122	Al_3	7.3554	7.0508
N_4	59.2200	255.8445	N_4	518.4328	1015.7500	N_4	89.0872	176.7298
Mn_5	1103.1944	682.7562	Mn_5	61898.6207	83180.6883	Mn_5	860.1968	607.8757
Ga_6	8.9005	7.1468	Ga_6	2.0906	109.3062	Ga_6	8.7556	6.9697
N_7	128.1480	149.7778	N_7	45.0158	440.5489	N_7	146.5804	115.6052
Ga_8	10.6774	8.0754	Ga_8	5.6210	31.7011	Al_8	9.1447	9.2445
N_9	41.8262	220.7655	N_9	445.6927	929.9371	N_9	97.5588	202.5538
N_{10}	1008.9373	1461.3802	N_{10}	3715.8543	8298.3128	N_{10}	1048.8518	1558.0300
Ga_{11}	4.0487	15.5383	Ga_{11}	0.2483	102.0391	Ga_{11}	3.0958	15.6767
N_{12}	120.7217	362.2518	N_{12}	367.1035	1288.8994	N_{12}	94.3074	348.4218
Ga_{13}	2.2765	25.1952	Ga_{13}	35.1872	123.5145	Al_{13}	4.1183	27.4952
N_{14}	1007.7725	1458.0491	N_{14}	1857.1102	7832.5114	N_{14}	1063.7258	1561.8895
Ga_{15}	4.0563	15.5221	Ga_{15}	11.5119	73.3284	Ga_{15}	3.0675	15.6962
N_{16}	120.6766	305.8095	N_{16}	655.7327	1345.8956	N_{16}	119.1640	317.7316
N_{17}	180.8583	320.6671	N_{17}	1055.9230	1712.1127	N_{17}	171.0876	325.8904
—	—	—	H_{18}	40.6176	502.4079	—	—	—

Continuation **TABLE 2.**

Mn@AlGaN–H			Mn@InGaN			Mn@InGaN–H		
Atom	σ_{iso}	σ_{aniso}	Atom	σ_{iso}	σ_{aniso}	Atom	σ_{iso}	σ_{aniso}
Ga_1	9.4127	57.4573	Ga_1	9.8561	9.0718	Ga_1	1.6742	42.3400
N_2	523.2930	1969.3799	N_2	141.2874	139.242	N_2	43.0241	535.2459
Al_3	3.9293	125.8000	In_3	10.6228	6.0792	In_3	16.1328	137.0235
N_4	1362.4308	2433.1374	N_4	70.7476	185.3866	N_4	1588.0044	3484.4781
Mn_5	44890.8709	68750.2634	Mn_5	1100.8028	655.478	Mn_5	75829.2468	87460.2786
Ga_6	14.4225	140.9499	Ga_6	8.0587	6.4922	Ga_6	12.6556	135.7235
N_7	367.1748	1905.4354	N_7	138.2746	141.262	N_7	190.1028	374.0311
Al_8	1.3642	33.6753	In_8	11.5107	8.9599	In_8	3.9630	42.2998
N_9	1645.6588	2817.2566	N_9	76.7525	215.6169	N_9	105.9158	687.9281
N_{10}	2093.5030	9430.3119	N_{10}	1078.6734	1612.3978	N_{10}	6052.6589	10061.7128
Ga_{11}	33.2386	113.4686	Ga_{11}	2.4981	16.2989	Ga_{11}	52.0566	69.7265
N_{12}	610.2133	1774.9398	N_{12}	101.3662	375.9026	N_{12}	883.0356	2354.1239
Al_{13}	10.8519	248.5418	In_{13}	0.6973	25.46	In_{13}	17.9037	85.9004
N_{14}	3210.8323	7998.7947	N_{14}	1134.3858	1669.9935	N_{14}	11759.9230	18294.7406
Ga_{15}	26.8216	118.0277	Ga_{15}	1.9593	16.6879	Ga_{15}	87.7874	114.0007
N_{16}	336.4981	1962.7560	N_{16}	129.6965	346.1977	N_{16}	123.9797	695.5940
N_{17}	498.3192	5128.1686	N_{17}	189.0956	365.8149	N_{17}	216.7121	726.1410
H_{18}	26.2759	347.0249	—	—	—	H_{18}	91.2315	651.1319

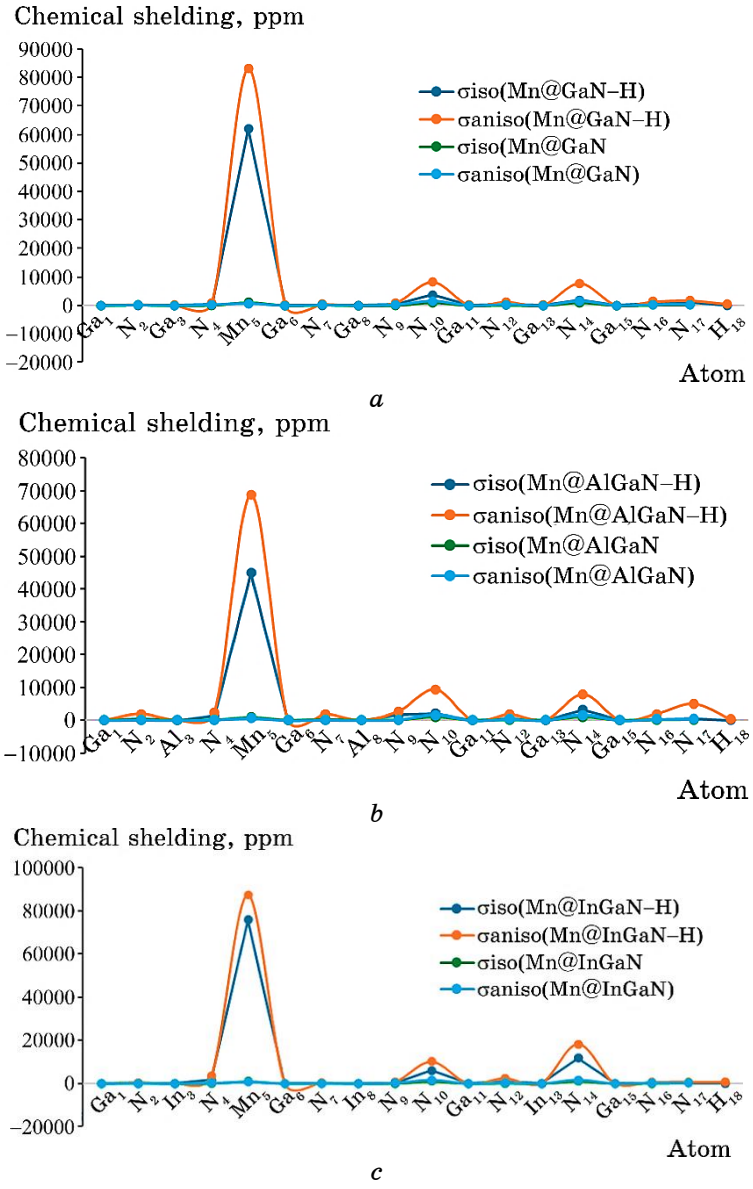

Fig. 6. The NMR spectra for heteroclusters of (*a*) Mn@GaN/Mn@GaN–H, (*b*) Mn@AlGaN/Mn@AlGaN–H, and (*c*) Mn@InGaN/Mn@InGaN–H.

The yield of electromagnetic shifting can be directed by the mentioned active nitrogen atoms extracted from hybrid nanomaterials. Therefore, it can be observed that doped heteroclusters of Mn@GaN, Mn@AlGaN, or Mn@InGaN might ameliorate the capa-

bility of GaN-based nanocomposites in solar cells for energy storage.

3.3. Insight of Infrared Spectroscopy and Thermochemistry

The infrared spectroscopy (IR) has been performed for nanocomposites of Mn@GaN/Mn@GaN–H (Fig. 7, *a*, *a*′), Mn@AlGaN/Mn@AlGaN–H

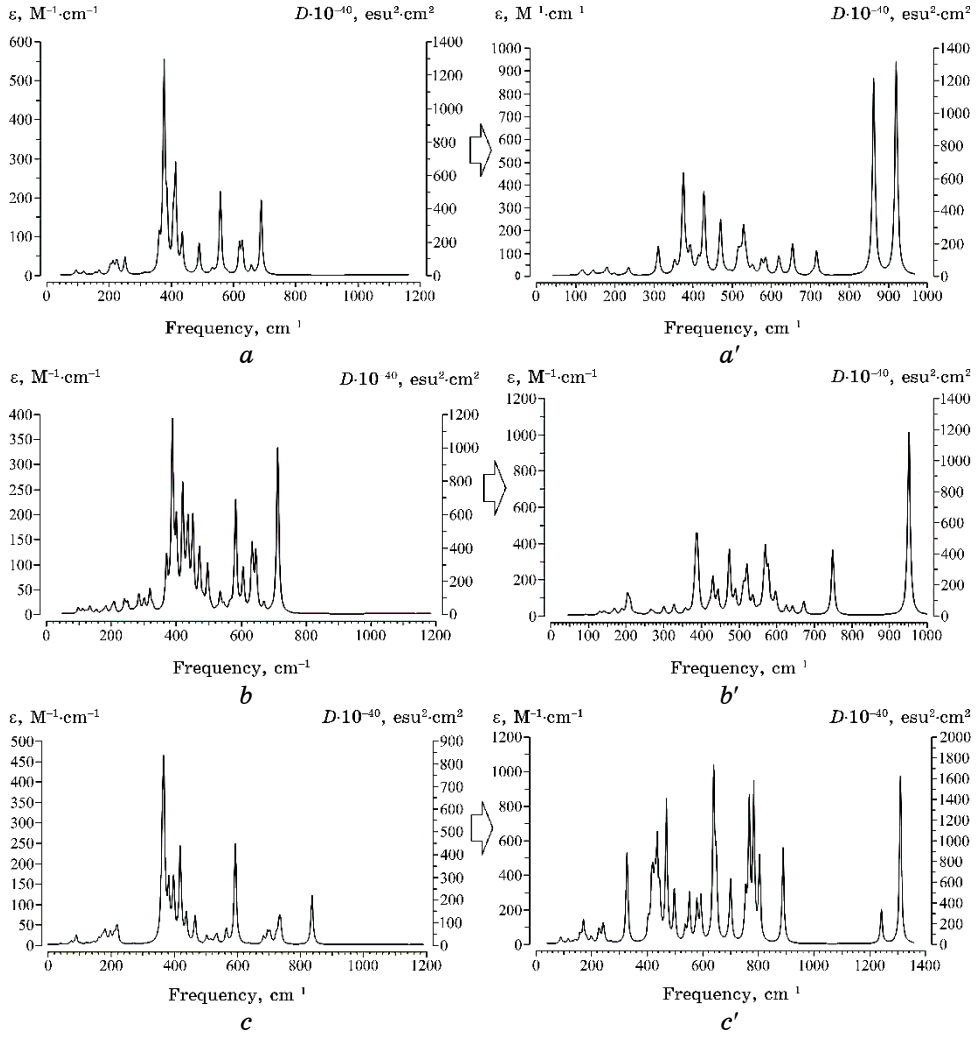

Fig. 7. The frequency (cm^{-1}) changes through the IR spectra for heteroclusters of (*a*) Mn@GaN/Mn@GaN–H, (*b*) Mn@AlGaN/Mn@AlGaN–H, and (*c*) Mn@InGaN/Mn@InGaN–H.

(Fig. 7, *b*, *b*′), and Mn@InGaN/Mn@InGaN–H (Fig. 7, *c*, *c*′) through hydrogen adsorption.

The frequency value through the IR curves between 200–1000 cm^{-1} for Mn@GaN with one sharp peak around 414.78 cm^{-1} (Fig. 7, *a*) has been shifted to two pointed peaks around 863.78 and 921.24 cm^{-1} of Mn@GaN–H (Fig. 7, *a*′). However, Figure 7, *b* shows two sharp peaks around 389.02 and 713.88 cm^{-1} for Mn@AlGaN that have been shifted to one sharp peak around 952.45 cm^{-1} for Mn@AlGaN–H (Fig. 7, *b*′). Furthermore, Figure 7, *c* indicates one sharp peak around 366.88 cm^{-1} for Mn@InGaN that have been shifted to several sharp peaks around 640.30, 767.66, 783.92, and 1311.73 cm^{-1} for Mn@InGaN–H (Fig. 7, *c*′).

Energy storage with heteroclusters has described that the frame of the overcoming cluster is related to Mn@GaN–H, Mn@AlGaN–H, and Mn@InGaN–H in the high amounts of frequency. This property makes these hybrid nanomaterials potentially advantageous for certain high-frequency applications requiring solar cells for energy storage. The advantages of manganese over GaN, AlGaN, or InGaN include its higher electron and hole mobility, allowing manganese doping devices to operate at higher frequencies than non-doping devices.

Table 3 through the thermodynamic specifications concluded that heteroclusters of Mn@GaN, Mn@GaN–H, Mn@AlGaN, Mn@AlGaN–H, Mn@InGaN, and Mn@InGaN–H might be more efficient structure for energy storage in the solar cells.

Thermodynamic parameters of heteroclusters of Mn@GaN/Mn@GaN–H, Mn@AlGaN/Mn@AlGaN–H, and Mn@InGaN/Mn@InGaN–H have been assigned (Table 3). The changes of Gibbs free energy versus for all nanocomposites could detect the maximum efficiency of Mn@AlGaN–H > Mn@GaN–H > Mn@InGaN–H for energy storage in the solar cells through ΔG_f^0 (Fig. 8).

The adsorption efficiency of Mn@GaN–H, Mn@AlGaN–H, Mn@InGaN–H based on dipole moment has been evaluated by the ΔG_f^0. The solar cells formed by Mn@GaN, Mn@AlGaN, Mn@InGaN feature a hierarchical structure with the electron donor/acceptor layer sandwiched by anode and cathode, which raises the importance of controlling the molecular crystal orientation, domain size, and vertical distribution to facilitate the charge collection at electrodes. In this paper, we have demonstrated that the nanocomposite semiconductor of gallium nitride-based structure can lead to a significant absorption enhancement in a broad spectral range of incident light in the presence of aluminium, indium and manganese. A comparison between solar cells containing 3*d* transition metal of Mn-doped GaN, AlGaN, InGaN shows that a solar cell containing these elements shows a more enhanced cell performance than the cells containing

TABLE 3. The thermodynamic characters of Mn@GaN, Mn@GaN–H, Mn@AlGaN, Mn@AlGaN–H, Mn@InGaN, Mn@InGaN–H nanoclusters using CAM–B3LYP–D3/6–311+G(*d*,*p*) calculation.

Compound	Dipole moment, Debye	$\Delta E^0_{ads}\cdot 10^{-3}$, kcal/mole	$\Delta H^0_{ads}\cdot 10^{-3}$, kcal/mole	$\Delta G^0_{ads}\cdot 10^{-3}$, kcal/mole	$E^0_{H\text{-binding}}$, kcal/mole
Mn@GaN	4.8247	–383.439	–383.439	–383.483	—
Mn@GaN–H	7.3741	–383.596	–383.595	–383.636	–157
Mn@AlGaN	4.7914	–383.095	–383.094	–383.136	—
Mn@AlGaN–H	7.3741	–383.596	–383.595	–383.636	–501
Mn@InGaN	7.3629	–383.035	–383.035	–383.082	—
Mn@InGaN–H	4.3037	–383.472	–383.472	–383.513	–437

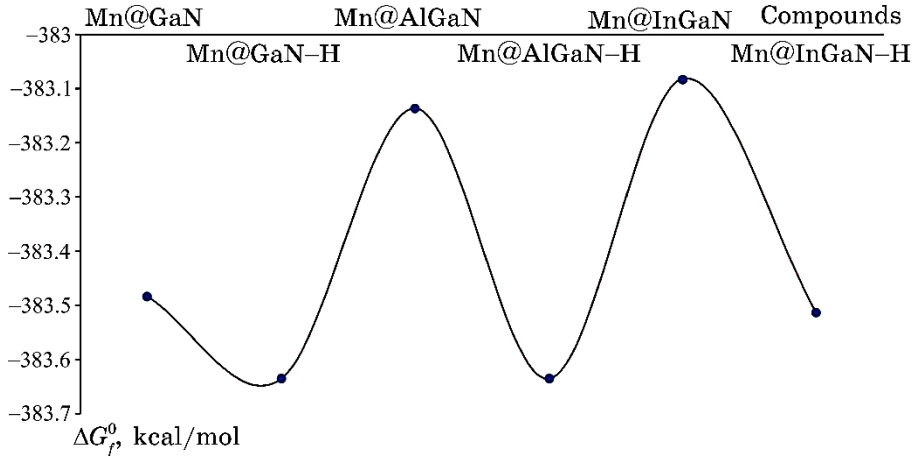

Fig. 8. Gibbs free energy, ΔG^0_f, for heteroclusters of Mn@GaN, Mn@GaN–H, Mn@AlGaN, Mn@AlGaN–H, Mn@InGaN, Mn@InGaN–H.

only the bare gallium nitride-based structure. This efficient doping strategy not only bridges the gaps of heteroatom doped GaN-based semiconductor materials, but also can provide deep insights into controlling the electrical and optical properties of these doping hybrid nanoclusters.

4. CONCLUSION

In summary, hydrogen grabbing on the heteroclusters of Mn-doped GaN, AlGaN, and InGaN as solar cells was investigated by first-principles calculations. We have provided gallium nitride-based semiconductors, which are doped with manganese. The geometrical

parameters of doping manganese on the surface of GaN, AlGaN, InGaN through the absorption status and current charge density of the solar cells were studied. Thermodynamic parameters have constructed a detailed molecular model for atom–atom interactions and a distribution of point charges, which can be utilized to reproduce the polarity of the solid material and the adsorbing molecules. Energy storage with heteroclusters has described that the frame of the overcoming cluster is related to Mn@GaN, Mn@AlGaN or Mn@InGaN in the high amounts of frequency. This property makes Mn@GaN, Mn@AlGaN or Mn@InGaN potentially advantageous for certain high-frequency applications requiring solar cells for energy storage due to hydrogen adsorption by formation of Mn@GaN–H, Mn@AlGaN–H or Mn@InGaN–H. The advantages of manganese over GaN, AlGaN, or InGaN include its higher electron and hole mobility, allowing manganese doping devices to operate at higher frequencies than non-doping devices. Thus, it should be explored its unique properties, such as its ability to increase energy storage which could lead to advancements solar cells.

ACKNOWLEDGEMENTS

In successfully completing this paper and its research, the authors is grateful to Kastamonu University.

REFERENCES

1. M. L. Nakarmi, N. Nepal, J. Y. Lin, and H. X. Jiang, *Appl. Phys. Lett*, **94**, Iss. 9: 091903 (2009); https://doi.org/10.1063/1.3094754
2. K. B. Nam, J. Li, M. L. Nakarmi, J. Y. Lin, and H. X. Jiang, *Appl. Phys. Lett.*, **84**, Iss. 25: 5264 (2004); https://doi.org/10.1063/1.1765208
3. J. P. Zhang, X. Hu, Y. Bilenko, J. Deng, A. Lunev, M. S. Shur, R. Gaska, M. Shatalov, J. W. Yang, and M. A. Khan, *Appl. Phys. Lett*, **85**, Iss. 23: 5532 (2004); https://doi.org/10.1063/1.1831557
4. Z. G. Shao, D. J. Chen, H. Lu, R. Zhang, D. P. Cao, W. J. Luo, Y. D. Zheng, L. Li and Z. H. Li, *IEEE Electron Device Lett.*, **35**, Iss. 25: 372 (2014); https://doi.org/10.1109/LED.2013.2296658
5. T. Kinoshita, T. Obata, H. Yanagi, and S.-I. Inoue, *Appl. Phys. Lett.*, **102**, Iss. 25: 012105 (2013); https://doi.org/10.1063/1.4773594
6. S. Liu, C. Ye, X. Cai, S. Li, W. Lin, and J. Kang, *Appl. Phys. A*, **122**, Iss. 5: 527 (2016); https://doi.org/10.1007/s00339-016-0073-0
7. John Simon, Vladimir Protasenko, Chuanxin Lian, Huili Xing, and Debdeep Jena, *Science*, **327**, Iss. 5961: 60 (2010); https://doi.org/10.1126/science.1183226
8. T. M. Al tahtamouni, J. Y. Lin, and H. X. Jiang, *AIP Adv*, **4**, Iss. 4: 047122 (2014); https://doi.org/10.1063/1.4871996
9. J.-K. Sheu, P.-C. Chen, C.-L. Shin, M.-L. Lee, P.-H. Liao, and W.-C. Lai,

Solar Energy Materials and Solar Cells, **157**, Iss. 6: 727 (2016); https://doi.org/10.1016/j.solmat.2016.07.047
10. J.-K. Sheu, F.-W. Huang, C.-H. Lee, M.-L. Lee, Y.-H. Yeh, P.-C. Chen, and W.-C. Lai, *Appl. Phys. Lett*, **103**, Iss. 6: 063906 (2013); https://doi.org/10.1063/1.4818340
11. A. Martí, C. Tablero, E. Antolín, A. Luque, R. P. Campion, and S. V. Novikov, and C. T. Foxon, *Solar Energy Materials and Solar Cells*, **93**, Iss. 5: 641(2009); https://doi.org/10.1016/j.solmat.2008.12.031
12. J. Wu, W. Walukiewicz, K. M. Yu, W. Shan, J. W. Ager, E. E. Haller, H. Lu, W. J. Schaff, W. K. Metzger, and S. Kurtz, *J. Appl. Phys*, **94**, Iss. 10: 6477 (2003); https://doi.org/10.1063/1.1618353
13. J. Wu, W. Walukiewicz, K. M. Yu, J. W. Ager, E. E. Haller, H. Lu, and W. J. Schaff, *Appl. Phys. Lett*, **80**, Iss. 25: 4741 (2002); https://doi.org/10.1063/1.1489481
14. R. Singh, D. Doppalapudi, T. D. Moustakas, and L. T. Romano, *Appl. Phys. Lett*, **70**, Iss. 9: 1089 (1997); https://doi.org/10.1063/1.118493
15. D.-H. Lien, Y.-H. Hsiao, S.-G. Yang, M.-L. Tsai, T.-C. Wei, S.-C. Lee, and J.-H. He, *Nano Energy*, **11**: 104 (2015); https://doi.org/10.1016/j.nanoen.2014.10.013
16. Y. Kuwahara, T. Fujii, Y. Fujiyama, T. Sugiyama, M. Iwaya, T. Takeuchi, S. Kamiyama, I. Akasaki, and H. Amano, *Appl. Phys. Express*, **3**, Iss. 11: 111001 (2010); https://doi.org/10.1143/APEX.3.111001
17. N. G. Young, R. M. Farrell, Y. L. Hu, Y. Terao, M. Iza, S. Keller, S. P. DenBaars, S. Nakamura, and J. S. Speck, *Appl. Phys. Lett.*, **103**, Iss. 17: 173903 (2013); https://doi.org/10.1063/1.4826483
18. C. J. Neufeld, S. C. Cruz, R. M. Farrell, M. Iza, J. R. Lang, S. Keller, S. Nakamura, S. P. DenBaars, J. S. Speck, and U. K. Mishra, *Appl. Phys. Lett.*, **98**, Iss. 24: 243507 (2011); https://doi.org/10.1063/1.3595487
19. H. Shen and B. Maes, *Opt. Express*, **19**, Suppl. 6: A1202 (2011); https://doi.org/10.1364/OE.19.0A1202
20. K. X. Wang, Z. Yu, V. Liu, Y. Cui, and S. Fan, *Nano Lett.*, **12**, Iss. 3: 1616 (2012); https://doi.org/10.1021/nl204550q
21. X. Meng, E. Drouard, G. Gomard, R. Peretti, A. Fave, and C. Seassal, *Opt. Express*, **20**, Iss. S5: A560 (2012); https://doi.org/10.1364/OE.20.00A560
22. A. Abass, K. Q. Le, A. Alu, M. Burgelman, and B. Maes, *Phys. Rev. B*, **85**, Iss. 11: 115449 (2012); https://doi.org/10.1103/PhysRevB.85.115449
23. R. Chriki, A. Yanai, J. Shappir, and U. Levy, *Opt. Express*, **21**, Iss. 103: A382 (2013); https://doi.org/10.1364/OE.21.00A382
24. W.-C. Hsu, J. K. Tong, M. S. Branham, Y. Huang, S. Yerci, S. V. Boriskina, and G. Chen, *Opt. Commun.*, **377**: 52 (2016); https://doi.org/10.1016/j.optcom.2016.04.055
25. O. Isabella, R. Vismara, A. Ingenito, N. Rezaei, and M. Zeman, *Opt. Express*, **24**, Iss. 6: A708 (2016); https://doi.org/10.1364/OE.24.00A708
26. J. Lin, Y. Yu, Z. Xu, F. Gao, Z. Zhang, F. Zeng, W. Wang, and G. Li, *J. Power Sources*, **450**: 227578 (2020); https://doi.org/10.1016/j.jpowsour.2019.227578
27. U. K. Kumawat, K. Kumar, P. Bhardwaj, and A. Dhawan, *Energy Science and Engineering*, **7**, Iss. 6: 2469 (2019); https://doi.org/10.1002/ese3.436
28. P. E. Blöchl, *Phys. Rev. B*, **50**, Iss. 24: 17953 (1994);

https://doi.org/10.1103/PhysRevB.50.17953
29. J. P. Perdew, K. Burke, and M. Ernzerhof, *Phys. Rev. Lett*, **77**, Iss. 24: 3865 (1996); https://doi.org/10.1103/PhysRevLett.77.3865
30. P. Ziesche, S. Kurth, and J. P. Perdew, *Comput. Mater. Sci.*, **11**: 122 (1998); https://doi.org/10.1016/S0927-0256(97)00206-1
31. M. Arrigoni and G. K. H. Madsen, *Comput. Mater. Sci.*, **156**: 354 (2019); https://doi.org/10.1016/j.commatsci.2018.10.005
32. P. Hohenberg and W. Kohn, *Phys. Rev. B*, **136**, Iss. 3B: B864 (1964); https://doi.org/10.1103/PhysRev.136.B864
33. W. Kohn and L. J. Sham, *Phys. Rev.*, **140**, Iss. 4A: A1133 (1965); https://doi.org/10.1103/PhysRev.140.A1133
34. A. D. Becke, *J. Chem. Phys.*, **98**, Iss. 7: 5648 (1993); https://doi.org/10.1063/1.464913
35. C. Lee, W. Yang, and R. G. Parr, *Phys. Rev. B*, **37**, Iss. 2: 785 (1988); https://doi.org/10.1103/PhysRevB.37.785
36. K. Kim and K. D. Jordan, *J. Phys. Chem*, **98**, Iss. 40: 10089 (1994); https://doi.org/10.1021/j100091a024
37. P. J. Stephens, F. J. Devlin, C. F. Chabalowski, and M. J. Frisch, *J. Phys. Chem.*, **98**, Iss. 45: 11623 (1994); https://doi.org/10.1021/j100096a001
38. F. Mollaamin and M. Monajjemi, *J. Clust. Sci.*, **34**, Iss .6: 2901 (2023); https://doi.org/10.1007/s10876-023-02436-5
39. F.Mollaamin and M. Monajjemi, *Int. J. Quantum Chem.*, **124**, Iss. 2: e27348 (2024); https://doi.org/10.1002/qua.27348
40. F. Mollaamin and M. Monajjemi, *Molecular Simulation*, **49**, Iss. 4: 365 (2023); https://doi.org/10.1080/08927022.2022.2159996
41. S. H. Vosko, L. Wilk, and M. Nusair, *Can. J. Phys.*, **58**, Iss. 8: 1200 (1980); https://doi.org/10.1139/p80-159
42. M. J. Frisch, G. W. Trucks, H. B. Schlegel, G. E. Scuseria, M. A. Robb, J. R. Cheeseman, G. Scalmani, V. Barone, G. A. Petersson, H. Nakatsuji, X. Li, M. Caricato, A. V. Marenich, J. Bloino, B. G. Janesko, R. Gomperts, B. Mennucci, H. P. Hratchian, J. V. Ortiz, A. F. Izmaylov, J. L. Sonnenberg, D. Williams-Young, F. Ding, F. Lipparini, F. Egidi, J. Goings, B. Peng, A. Petrone, T. Henderson, D. Ranasinghe, V. G. Zakrzewski, J. Gao, N. Rega, G. Zheng, W. Liang, M. Hada, M. Ehara, K. Toyota, R. Fukuda, J. Hasegawa, M. Ishida, T. Nakajima, Y. Honda, O. Kitao, H. Nakai, T. Vreven, K. Throssell, J. A. Montgomery, Jr., J. E. Peralta, F. Ogliaro, M. J. Bearpark, J. J. Heyd, E. N. Brothers, K. N. Kudin, V. N. Staroverov, T. A. Keith, R. Kobayashi, J. Normand, K. Raghavachari, A. P. Rendell, J. C. Burant, S. S. Iyengar, J. Tomasi, M. Cossi, J. M. Millam, M. Klene, C. Adamo, R. Cammi, J. W. Ochterski, R. L. Martin, K. Morokuma, O. Farkas, J. B. Foresman, and D. J. Fox, *Gaussian 16, Revision C.01* (Wallingford, CT: Gaussian, Inc.: 2016).
43. R. Dennington, T. A. Keith, and J. M. Millam, *GaussView, Version 6.06.16* (Shawnee Mission, KS: Semichem Inc.: 2016).
44. Z. Xu, C. Qin, Y. Yu, G. Jiang, and L. Zhao, *AIP Advances*, **14**, Iss. 8: 055114 (2024); https://doi.org/10.1063/5.0208082
45. A. D. Becke and K. E. Edgecombe, *J. Chem. Phys.*, **92**, Iss. 9: 5397 (1990); https://doi.org/10.1063/1.458517
46. S. N. Steinmann, Y. Mob, and C. Corminboeuf, *Phys. Chem. Chem. Phys.*,

13, Iss. 46: 20584 (2011); https://doi.org/10.1039/C1CP21055F
47. L. Tian and C. Fei-Wu, *Acta Phys. Chim. Sin.*, **27**, Iss. 12: 2786 (2011); https://doi.org/10.3866/PKU.WHXB20112786
48. A. Savin, O. Jepsen, J. Flad, O. K. Andersen, H. Preuss, and H. G. von Schnering, *Angew. Chem. Int. Edit. Engl.*, **31**, Iss. 2: 187 (1992); https://doi.org/10.1002/anie.199201871
49. U. Sohail, F. Ullah, N. H. Binti Zainal Arfan, M. H. S. Abdul Hamid, T. Mahmood, N. S. Sheikh, and K. Ayub, *Molecules*, **28**, Iss. 10: 4060 (2023); https://doi.org/10.3390/molecules28104060